J Solid State Electrochem (2017) 21:463–468
DOI 10.1007/s10008-016-3374-5

ORIGINAL PAPER

Electrochemically synthesized nanoporous gold as a cathode material for Li-O_2 batteries

Heng Yang[1] · **Jiaxin Xia**[2] · **Loriana Bromberg**[2] · **Nikolay Dimitrov**[1,2] · **M. Stanley Whittingham**[1,2]

Received: 4 August 2016 / Revised: 15 August 2016 / Accepted: 19 August 2016 / Published online: 8 September 2016

Abstract Nanoporous gold (NPG) prepared via chemical de-alloying has been recently shown to dramatically improve the reversibility and kinetics of Li-O_2 batteries, but high cost makes its use as practical electrode material difficult. Recently developed electrochemical routines for synthesis of very thin NPG layers (<100 nm) on various low-cost substrates could potentially provide a feasible economic alternative. In this work, NPG on both gold and glassy carbon (GC) substrates was successfully synthesized via electrochemical de-alloying method and tested as cathode material in Li-O_2 batteries. The results show that electrochemically synthesized NPG cathode cycles repeatedly with $LiFePO_4$ anode. The voltage hysteresis is also significantly reduced when NPG is used in comparison with plain GC. Along with these results, challenges that need to be addressed for future implementation of NPG cathode in practical Li-O_2 batteries are also discussed.

Keywords Li-O_2 battery · Nanoporous gold · Reversibility · Cyclic voltammetry

Electronic supplementary material The online version of this article (doi:10.1007/s10008-016-3374-5) contains supplementary material, which is available to authorized users.

✉ Heng Yang
hyang7@binghamton.edu

✉ M. Stanley Whittingham
stanwhit@gmail.com

[1] Materials Science and Engineering Program, The State University of New York at Binghamton, Binghamton, NY 13902-6000, USA

[2] Department of Chemistry, The State University of New York at Binghamton, Binghamton, NY 13902-6000, USA

Introduction

Li-O_2 batteries have been under intensive studies for the past few years due to their highest theoretical energy density among all secondary battery systems [1–4]. The development of a Li-O_2 battery, however, is hindered by great challenges including but not limited to (1) identifying electrolyte and electrode materials that would be stable in the presence of lithium oxides, in particular lithium superoxide (LiO_2) [5]; (2) developing bifunctional electrocatalysts to reduce the large voltage hysteresis (very low energy efficiency) [6, 7]; (3) improving reaction kinetics [8–10]; and (4) protecting the lithium anode and addressing lithium dendrite issues [11–13]. Recently, Peng et al. [8] demonstrated that fast and reversible cycling of Li-O_2 batteries is possible by using nanoporous gold (NPG) as the cathode material synthesized by chemical de-alloying of Ag-Au alloy along with dimethyl sulfoxide (DMSO) as the electrolyte solvent. However, the NPG electrodes used in reference [8] are relatively thick and therefore expensive to implement. A way to address this issue could be the use of a recently developed all-electrochemical method [14] that enables the fabrication of very thin NPG films, on both gold and carbon surfaces, thus providing a viable cost-effective alternative. Processed accordingly, ultrathin NPG films feature ligament and pore sizes in the single-digit nanometer range [15] and can additionally be fine-tuned to improve the performance in specific applications [15–17]. Therefore, exploiting advantages of these developments, the work presented herein emphasizes an implementation, systematic testing, and investigation of the properties of NPG thin films fabricated on Au and glassy carbon (GC) substrates as cathode materials for Li-O_2 batteries.

Experimental

Lithium disks (1.91 cm^2, 0.25 mm thick) were purchased from MTI and used as counter and reference electrodes. In galvanostatic cycling tests, $LiFePO_4$ electrodes were used as anodes (counter and reference electrodes) owing to their excellent chemical stability. The $LiFePO_4$ electrodes were prepared by casting slurry onto aluminum foil. The slurry was prepared by mixing $LiFePO_4$ powder (Primet Inc.), carbon powder (Super C65, Timcal), and polyvinylidene fluoride (PVDF, Aldrich) in an 8:1:1 weight ratio, followed by ball-milling for 5 min.

Lithium hexafluorophosphate ($LiPF_6$, Aldrich) of 0.1 M concentration in DMSO (Aldrich, ≥99.9 %) was prepared in an argon-filled glovebox. Lithium bis (trifluoromethane) sulfonimide (LiTFSI) of 1 M concentration in tetraethylene glycol dimethyl ether (TEGDME) was purchased from BASF Company with a certified moisture level (20 ppm maximum; 10 ppm analysis).

Electrochemical fabrication of NPG on Au and GC substrate followed protocols developed in our previous publications [14, 15, 17, 18]. A brief summary of the fabrication and characterization of a NPG electrode is presented in the electronic supplemental material (Fig. S1–S4 and Table S1). The morphology of the NPG samples was analyzed by a Supra 55 FESEM (Zeiss).

The as-prepared tablets with very thin NPG film on top were assembled with one piece of lithium or $LiFePO_4$ anode, glass fiber separator (Whatman, GF/B), and Celgard separator, followed by the addition of 200 μL electrolyte. The cell components were pressed together by a spring inside a stainless steel cell body, which was assembled and sealed inside the glovebox and connected to a gas line before testing [19]. Helium or oxygen gas was first dried by a Drierite Gas Purifier and then purged through the cell for at least 30 min before each electrochemistry measurement, which was carried out with a MPG2 potentiostat with EC lab software (Bio-Logic Science Instrument). The open circuit voltage (OCV) of the cells studied in the present work fell in the range of 2.9 to 3.3 V (versus Li^+/Li). For the cyclic voltammetry (CV) measurements, the potential was first scanned in the positive direction (anodic), as a routine procedure to check the background current level prior to the oxygen reduction reaction in the reverse scan.

Results and discussion

The morphology and structure of as-synthesized NPG on Au substrate can be found in our previous publication [15]. Figure 1a shows the SEM image taken after 300 CV cycles at various scan rates in TEGDME-based electrolyte. It can be clearly seen that no structure damage occurred during the cycling. The NPG film features an interconnected solid-void 3D structure [16], with ligament and pore size in the dimension of around 15~30 nm. As mentioned earlier, the de-alloying process may be fine-tuned to ensure 5- to 40-fold surface area development, accommodating needs of specific applications. In this work, the surface area of the NPG/Au cathode (see Fig. 1a) is 5.19 cm^2, as determined by a Pb underpotential deposition (UPD) method [18]. This is 6.6 times larger than the polished bulk Au tablet featuring a physical surface area of 0.785 cm^2. The current density calculations in this paper, however, are based on the physical surface area of flat Au (0.785 cm^2) and GC (0.196 cm^2) tablets, for direct comparison between flat and developed NPG surfaces.

The NPG/Au sample was first assessed by CV with a Li anode and 0.1 M $LiPF_6$/DMSO electrolyte. The featureless CV curves presented as dotted lines in Fig. 1b imply an electrochemically inert environment realized by purging the cell with He for both bulk Au and NPG/Au electrodes. Switching to purging with oxygen apparently enables the oxygen reduction reaction (ORR, Li_2O_2 formation in the cathodic scan) and oxygen evolution reaction (OER, Li_2O_2 decomposition in the anodic scan). While both reactions are initiated around the thermodynamic potential (2.96 V vs. Li^+/Li), the reduction peak (E_{pc}) and the oxidation peak (E_{pa}) emerge at c.a. 2.5 and 3.3 V, respectively. Expectedly, NPG/Au exhibits markedly higher ORR and OER activity than a bulk Au electrode, which is propelled by the 6.6-fold surface area increase as a result of the NPG fabrication. The improvement becomes much more obvious on OER (blue curve, anodic scan) as the counterpart bulk Au electrode (red solid line) produces a practically flat anodic curve indicating lack of reversibility. It is noteworthy that the insufficiency or lack of OER product (preferably Li_2O_2) was mainly observed at a slow scan rate, whereby presumably the time scan duration (c.a. 800 s per cycle at 5 mV/s) is too long for the ORR products to build up and eventually bind to the flat Au surface. In addition, clearly confirming the kinetic nature of the observed phenomenology, the total anodic charge for NPG/Au is only one third of the cathodic charge (as calculated from the integrated area under ORR and OER peaks). We infer from these results that the NPG structure is essential for binding to and thus for eventually retaining the ORR products. In the longer run, however, the NPG structure might require further adjustment, i.e., surface coarsening, to improve the pore-filling efficiency of Li_2O_2.

Figure 2a shows the discharge/charge curves for up to five cycles in a cell assembled with a $LiFePO_4$ anode, NPG/Au cathode, and 0.1 M $LiPF_6$/DMSO electrolyte. In this case, a $LiFePO_4$ anode was employed instead of lithium anode because of its excellent chemical stability. The use of $LiFePO_4$ electrode as the lithium source for Li-O_2 batteries has been demonstrated previously [9, 19].

The thickness of the deposited NPG is calculated to be 74 nm (Table S1). A conservative estimate of a void space

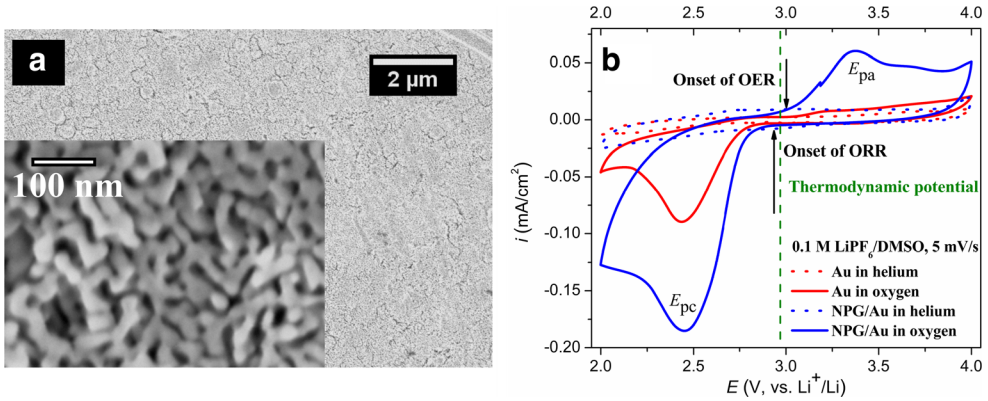

Fig. 1 **a** SEM image of NPG/Au and **b** CV curves of Au and NPG/Au tested with 0.1 M $LiPF_6$/DMSO electrolyte and helium or oxygen gas purging

volume of 1.96×10^{-6} cm^3 is made for a NPG film with 50 nm thickness and 50 % void space. Such void volume theoretically accommodates 4.53×10^{-6} g of Li_2O_2 based on the density of Li_2O_2 (2.31 g cm^{-3}), which leads to a calculated electrochemical capacity of 0.0054 mAh. Therefore, given the total volume of $2 \times 1.96 \times 10^{-6}$ cm^3, the volumetric capacity could be calculated to be 1380 mAh cm^{-3}. Since the deposited Au mass is 1.08×10^{-5} g (see Table S1), the gravimetric capacity should be 501 mAh g^{-1} based on the total NPG film mass. Notably, this structural estimate assumes 100 % pore-filling efficiency of Li_2O_2 in the NPG void space, which is clearly not the case, as the following discussion elaborates in more detail.

As shown in Fig. 2a, the discharge was terminated when a capacity of 0.0054 mAh was reached, so that all the pores of the NPG would be presumably filled with Li_2O_2. Because of the much larger capacity of the $LiFePO_4$ electrode (~0.3 mAh), the voltage response is assumed to be correlated with the reactions taking place at the NPG cathode. The conversion to a lithium scale is made for direct comparison. The discharge curve in the first cycle exhibits sloped potential response in the early stage (up to ~2 μAh), which gradually reaches a plateau at around 2.75 V vs. Li$^+$/Li. This behavior is probably related to the increasing resistance of ORR products that accumulate in the pores of NPG. The flat discharge curve towards the end of cutoff capacity indicates that the NPG

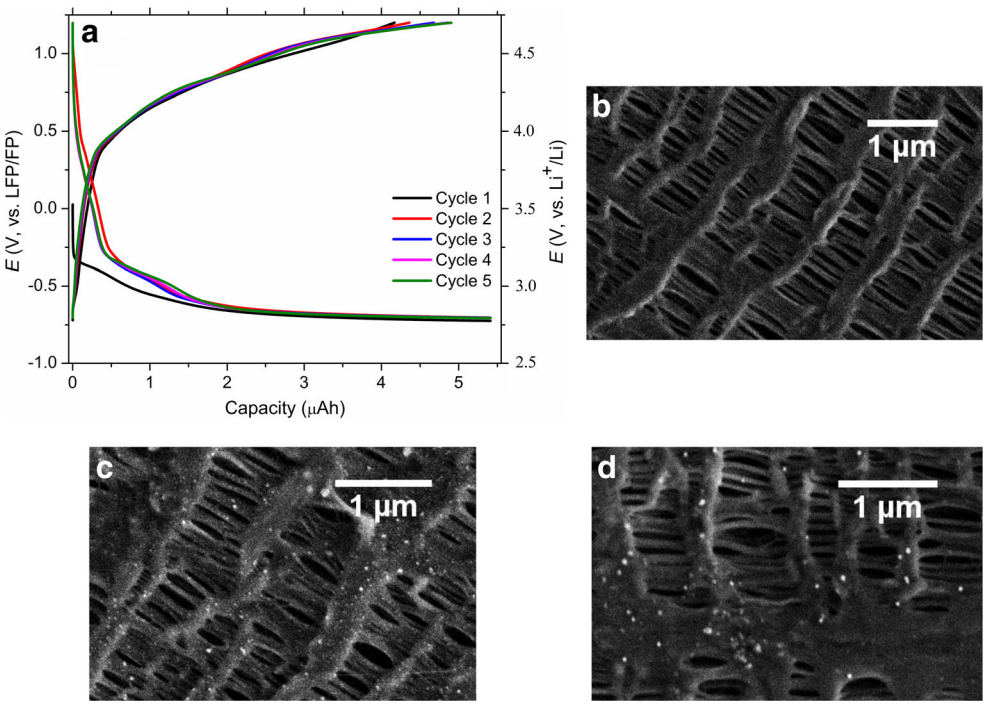

Fig. 2 **a** Discharge and charge curves of NPG/Au with $LiFePO_4$ anode at 5.19 μA (1 μA/cm^2 based on actual surface area determined by Pb UPD) and SEM images of **b** the Celgard separator, and the Celgard separators in contact with NPG/Au cathode after **c** discharge and **d** charge with a $LiFePO_4$ anode. Electrochemical tests were conducted with 0.1 M $LiPF_6$/DMSO electrolyte and O_2 gas purging

surface is still active and is able to sustain further ORR. In the charge segment, the potential gradually increases, in association with the decreasing content of ORR products. Starting from the second cycle, approximately 1 μAh discharge capacity is obtained above the thermodynamic potential of ORRs (2.96 V vs. Li for Li_2O_2 formation in nonaqueous electrolyte), which hints at the presence of side reactions and will be discussed later (see Fig. 3).

Upon dissembling the cells at the end of electrochemical tests, we observed color change (from white to black) in the area where the Celgard separator was in contact with the NPG/Au electrode. The separators after discharge and charge were then examined by SEM (Fig. 2b~d). Nano-sized particles were found on the separator's surface after discharge. After charge, the density of those particles was noticeably smaller but they were still present at measurable levels. This indicates that some of these particles were not in direct contact with the catalytically active Au surface and therefore could not be oxidized.

In previous studies associated with a Au cathode, free-standing NPG films [8, 9] or Au microlattice [20] were employed so that oxygen could diffuse through the back of the electrode and Li_2O_2 could be formed right where the three phases, oxygen/Au/electrolyte, meet and react. In the present study, the NPG layer is deposited on a solid Au or GC substrate which prevents oxygen diffusion from the back side of the electrodes. Instead, the ORR takes place at the Au/electrolyte interface with dissolved oxygen and possibly superoxide species formed during discharge [21]. On the other hand, mass transport within the interconnected nanosized channels may not be fast enough [18], especially when the concentration of dissolved oxygen or superoxide species is low. These factors lead to part of the ORR taking place near the topmost surface of the NPG electrode, thus reducing the pore-filling efficiency. This kind of remote deposition/immobilization of ORR products could in part explain the disproportionally small OER peak (Fig. 1b) and the insufficient charging process (Fig. 2a). That same issue might also be the cause for the higher voltage hysteresis shown in Fig. 2a in comparison with reference [8].

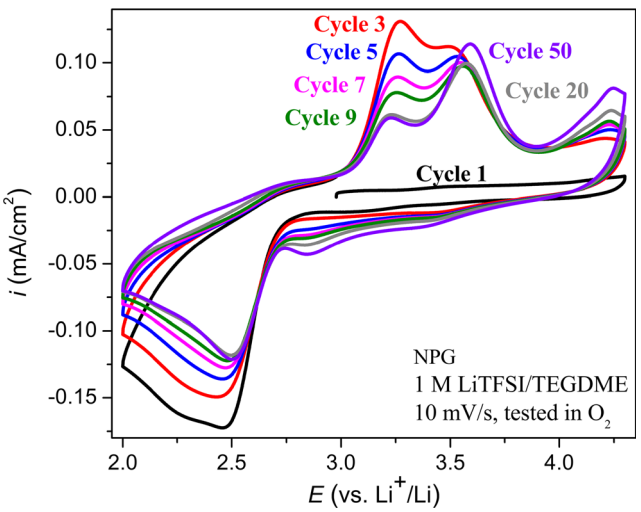

Fig. 3 CV curves of NPG/Au in 1 M LiTFSI/TEGDME at 10 mV/s for 50 cycles

These challenges make very difficult the extensive testing of the NPG electrodes with constant current charge/discharge cycles. Nevertheless, the main objective of the present study is to discuss the feasibility of employing an electrochemically synthesized NPG on Au and low-cost carbon surface for Li-O_2 batteries, as well as to reveal the nature of the electrochemical reactions at the NPG/electrolyte interface. In the future, oxygen diffusion channels might need to be added if a solid substrate was used. Ideally, the NPG layer could be synthesized directly on porous substrate.

Interestingly, in support of our earlier discussion, a very recent publication reported a solution phase discharge of Li-O_2 batteries, in which case Li_2O_2 does not deposit into the pores of the electrode [22]. The NPG architectures developed in our work may be promising electrodes employed along with this reaction route, considering the enhanced chemical stability and kinetics compared with carbon electrodes.

Figure 3 presents the CV curves of NPG/Au in 1 M LiTFSI/TEGDME electrolyte for up to 50 cycles at a sweep rate of 10 mV/s. The ORR and OER peaks positioned at around 2.5 and 3.3 V, respectively, are similar to those shown with the CV curve in Fig. 1b. During the CV cycles in this case, however, the ORR and OER peaks show gradual reduction in the peak current density, which was reported earlier and was attributed to surface passivation [23]. A second pair of peaks appears at 3.5 V (anodic) and 2.8 V (cathodic) after the first cycle, and interestingly, current densities of these new peaks increase with the number of cycles. It is important to note that this pair of peaks is completely absent in the first cycle; therefore, the existence of these peaks may be related to the accumulation of ORR products on the Au surface. In fact, a similar phenomenology attributed to the behavior of Au in aprotic electrolyte was documented by Aurbach et al. in [24] whereby this new pair of peaks was evidently related to Au hydroxide formation/decomposition in the presence of LiOH. The presence of LiOH, which is possibly hydrated, is required for a local high-pH environment so that Au oxidation reaction is feasible at such a relatively negative potential (see also Pourbaix diagram [25]). In our studies, LiOH could emerge as a result of a secondary chemical reaction of Li_2O_2 with traces of moisture in the system, mostly from the electrolyte and/or the gas supply. This Au oxidation/reduction reaction explains the capacity obtained beyond the thermodynamic potential range (Fig. 2a). However, this redox transition of the Au surface seems to be reversible, and as such, it would

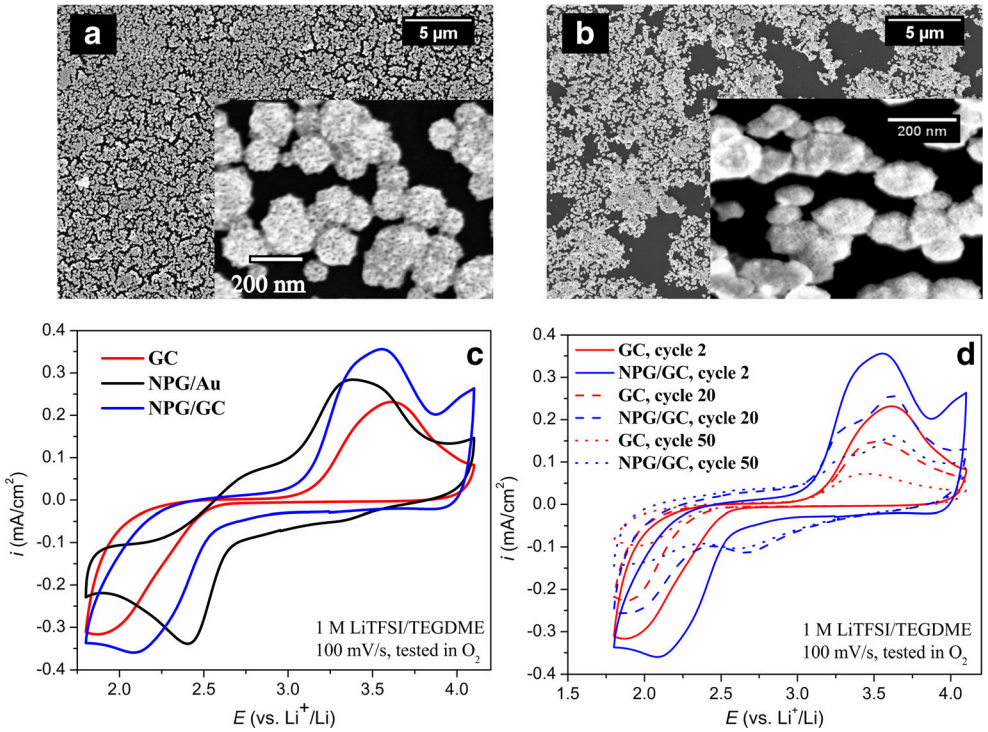

Fig. 4 SEM image of NPG/GC **a** prior to CV test and **b** after CV test; **c** CV curves of GC, NPG/Au, and NPG/GC at 100 mV/s (second cycle); and **d** CV curves of GC and NPG/GC at 100 mV/s (2nd, 20th, and 50th cycles)

not affect the kinetics of the following discharge/charge cycles.

Compared to NPG/Au (Fig. 1a), NPG on GC substrate typically features isolated clusters of nanoporous gold on the surface [17]. The size of the NPG clusters shown in Fig. 4a ranges from 10 to 200 nm, with the majority of the clusters featuring the size of 100~150 nm. Figure 4b shows the morphology of the NPG/GC electrode after 100 CV cycles at 100 mV/s. Although the porous structure on each cluster is retained, the general deposit morphology is somewhat altered. Most likely, this alteration took place during the cell assembly and numerous CV tests. This suggests that the adhesion of NPG on GC substrate is much weaker than that on Au substrate. Addressing similar issues recently, we developed and demonstrated elsewhere means for significant improvement of the adhesion of NPG on GC substrate [26, 27].

Figure 4c shows the second cycle of CV tests for polished flat GC, NPG/Au, and NPG/GC at a scan rate of 100 mV/s. The ORR onset and peak potential position is in the order of $E_{GC} < E_{NPG/GC} < E_{NPG/Au}$ whereas the order is reversed during OER. This shows that both NPG and unshielded GC substrate affect the ORR and OER behavior, and the NPG significantly reduces the voltage hysteresis in comparison with a flat GC. A fabrication of recently reported [28] continuous layer of NPG on GC may further reduce the voltage hysteresis making it closer to that obtained by NPG/Au.

Figure 4d shows the CV curves of GC and NPG/GC for the 2nd, 20th, and 50th cycles at 100 mV/s. While only one pair of ORR and OER peaks could be observed on GC only, an additional pair of peaks can be clearly seen at similar positions as shown in Fig. 3 for NPG/Au. This provides further evidence that Au is repeatedly oxidized and reduced with the scans.

Conclusion and outlook

NPG/Au and NPG/GC were successfully synthesized using all electrochemical fabrication routines and tested as Li-O_2 battery cathodes. The morphology of NPG/Au shows a continuous interconnected solid-void 3D structure, in contrast to the isolated NPG clusters on the GC surface. CV and galvanostatic discharge/charge tests showed that the voltage hysteresis is greatly reduced compared with carbon electrode. Also, the electrochemically synthesized NPG cathode can cycle repeatedly in oxygen environment. We observed Au oxidation/reduction behavior in the presence of moisture traces, but this reaction appears to be reversible. Future work on adjusting the NPG ligament-pore size ratio and providing oxygen diffusion channels may improve the pore-filling efficiency of ORR products. Most importantly, we demonstrated that NPG deposits could be conveniently synthesized on both Au and low-cost carbon surface via electrochemical routes, which could lead to a cost-effective application of NPG electrodes in batteries and fuel cells.

Acknowledgments This research is supported by the New York State Energy Research Development Authority [NYSERDA] under Agreement No. 18500. Partial support is also provided by the National Science Foundation, Division of Chemistry, CHE-1310297. The authors are grateful to the help and fruitful discussions from Mr. George Shovlowsky, Mr. Bob Gonzales, and Dr. Natalya Chernova (Binghamton University).

References

1. Abraham KM, Jiang Z (1996) A polymer electrolyte-based rechargeable lithium/oxygen battery. J Electrochem Soc 143:1–5
2. Girishkumar G, McCloskey B, Luntz AC, Swanson S, Wilcke W (2010) Lithium–air battery: promise and challenges. J Phys Chem Lett 1:2193–2203
3. Ogasawara T, Débart A, Holzapfel M, Novák P, Bruce PG (2006) Rechargeable Li_2O_2 electrode for lithium batteries. J Am Chem Soc 128:1390–1393
4. Whittingham MS (2012) History, evolution, and future status of energy storage. Proc IEEE 100:1518–1534
5. McCloskey BD, Speidel A, Scheffler R, Miller DC, Viswanathan V, Hummelshøj JS, Nørskov JK, Luntz AC (2012) Twin problems of interfacial carbonate formation in nonaqueous Li–O_2 batteries. J Phys Chem Lett 3:997–1001
6. McCloskey BD, Scheffler R, Speidel A, Bethune DS, Shelby RM, Luntz AC (2011) On the efficacy of electrocatalysis in nonaqueous Li-O_2 batteries. J Am Chem Soc 133:18038–18041
7. Harding JR, Lu Y-C, Tsukada Y, Shao-Horn Y (2012) Evidence of catalyzed oxidation of Li_2O_2 for rechargeable Li-air battery applications. Phys Chem Chem Phys 14:10540–10546
8. Peng Z, Freunberger SA, Chen Y, Bruce PG (2012) A reversible and higher-rate Li-O_2 battery. Science 337:563–566
9. Chen Y, Freunberger SA, Peng Z, Fontaine O, Bruce PG (2013) Charging a Li-O_2 battery using a redox mediator. Nat Chem 5:489–494
10. Lu Y-C, Gallant BM, Kwabi DG, Harding JR, Mitchell RR, Whittingham MS, Shao-Horn Y (2013) Lithium-oxygen batteries: bridging mechanistic understanding and battery performance. Energy Environ Sci 6:750–768
11. Kim H, Jeong G, Kim Y-U, Kim J-H, Park C-M, Sohn H-J (2013) Metallic anodes for next generation secondary batteries. Chem Soc Rev 42:9011–9034
12. Xu W, Wang JL, Ding F, Chen XL, Nasybutin E, Zhang YH, Zhang JG (2014) Lithium metal anodes for rechargeable batteries. Energy Environ Sci 7:513–537
13. Yang H, Fey EO, Trimm BD, Dimitrov N, Whittingham MS (2014) Effects of pulse plating on lithium electrodeposition, morphology and cycling efficiency. J Power Sources 272:900–908
14. McCurry DA, Kamundi M, Fayette M, Wafula F, Dimitrov N (2011) All electrochemical fabrication of a platinized nanoporous Au thin-film catalyst. ACS Appl Mater Interfaces 3:4459–4468
15. Kamundi M, Bromberg L, Fey E, Mitchell C, Fayette M, Dimitrov N (2012) Impact of structure and composition on the dealloying of $Au_xAg_{(1-x)}$ alloys on the nanoscale. J Phys Chem C 116:14123–14133
16. Erlebacher J, Aziz MJ, Karma A, Dimitrov N, Sieradzki K (2001) Evolution of nanoporosity in dealloying. Nature 410:450–453
17. Kamundi M, Bromberg L, Ogutu P, Dimitrov N (2013) Seeding strategies for the deposition of high density network of nanoporous Au cluster catalyst on glassy carbon electrodes. J Appl Electrochem 43:879–890
18. Liu Y, Bliznakov S, Dimitrov N (2009) Comprehensive study of the application of a Pb underpotential deposition-assisted method for surface area measurement of metallic nanoporous materials. J Phys Chem C 113:12362–12372
19. Yang H, Wang Q, Zhang R, Trimm BD, Whittingham MS (2016) The electrochemical behaviour of TTF in Li-O_2 batteries using a TEGDME-based electrolyte. Chem Commun 52:7580–7583
20. Xu C, Gallant BM, Wunderlich PU, Lohmann T, Greer JR (2015) Three-dimensional Au microlattices as positive electrodes for Li–O_2 batteries. ACS Nano 9:5876–5883
21. Johnson L, Li C, Liu Z, Chen Y, Freunberger SA, Ashok PC, Praveen BB, Dholakia K, Tarascon J-M, Bruce PG (2014) The role of LiO_2 solubility in O_2 reduction in aprotic solvents and its consequences for Li–O_2 batteries. Nat Chem 6:1091–1099
22. Gao X, Chen Y, Johnson L, Bruce PG (2016) Promoting solution phase discharge in Li-O_2 batteries containing weakly solvating electrolyte solutions. Nat Mater 15:882–888
23. Trahan MJ, Mukerjee S, Plichta EJ, Ma H, Abraham KM (2012) Studies of Li-air cells utilizing dimethyl sulfoxide-based electrolyte. J Electrochem Soc 160:A259–A267
24. Aurbach D, Daroux M, Faguy P, Yeager E (1991) The electrochemistry of noble metal electrodes in aprotic organic solvents containing lithium salts. J Electroanal Chem 297:225–244
25. Pourbaix M (1974) Atlas of electrochemical equilibria in aqueous solutions. National Association of Corrosion Engineers, Houston
26. Bromberg L, Xia J, Rooney R, Dimitrov N (2014) Enhanced adhesion of continuous nanoporous Au layers by thermochemical oxidation of glassy carbon. Coatings 4:416–432
27. Xia J, Rooney R, Ambrozik S, Bromberg LA, Dimitrov N (2015) Enhanced adhesion of ultrathin nanoporous Au deposits by electrochemical oxidation of glassy carbon. J Electrochem Soc 162:H308–H316
28. Bromberg LA, Xia J, Fayette M, Dimitrov N (2014) Synthesis of ultrathin and continuous layers of nanoporous Au on glassy carbon substrates. J Electrochem Soc 161:D3001–D3010